Geomechanics and Engineering, *Vol. 18, No. 5 (2019) 555-566*
DOI: https://doi.org/10.12989/gae.2019.18.5.555

Influence of temperature on the beams behavior strengthened by bonded composite plates

Mokhtar Bouazza*[1,2], Kamel Antar[2], Khaled Amara[2,3], Samir Benyoucef[2,4] and El Abbes Adda Bedia[5]

[1]*Department of Civil Engineering, University of Tahri Mohamed of Bechar, 08000, Algeria*
[2]*Laboratory of Materials and Hydrology, University of Sidi Bel Abbes, 22000, Algeria*
[3]*Department of Civil Engineering, University Centre of Ain Temouchent, 46000, Algeria*
[4]*Department of Civil Engineering, University of Sidi Bel Abbes, 22000, Algeria*
[5]*Centre of Excellence for Advanced Materials Research, King Abdulaziz University, Jeddah, 21589, Saudi Arabia*

(Received April 13, 2019, Revised July 2, 2019, Accepted July 15, 2019)

Abstract. The purpose of this paper is to investigate the thermal effects on the behaviour reinforced-concrete beams strengthened by bonded angle-ply laminated composites laminates plate $[\pm\theta n/90m]_S$. Effects of number of 90° layers and number of ±θ layers on the distributions of interfacial stress in concrete beams reinforced with composite plates have also been studied. The present results represent a simple theoretical model to estimate shear and normal stresses. The effects the temperature, mechanical properties of the fibre orientation angle of the outer layers, the number of cross-ply layers, plate length of the strengthened beam region and adhesive layer thickness on the interfacial shear and normal stresses are investigated and discussed.

Keywords: interfacial stresses; concrete beam; angle-ply laminates; fibre angle

1. Introduction

Reinforced concrete (RC) beams or metallic beams can be strengthened by bonding steel or composite plates/sheets to tension surfaces (Taljsten 1997, Roberts and Haji-Kazemi 1989, Oehlers *et al.* 1997, Malek *et al.* 1998, Smith and Teng 2001, Teng *et al.* 2001, Roberts 2001, Fragiacomo 2005, Tounsi 2006, Qiao and Chen 2008, Narayanamurthy et al 2010,2011,2016, Hoque *et al.* 2007, Siu and Su 2011, Kara and Dundar 2012). Shear strengthening of reinforced concrete beams with rectangular web openings by FRP composites was studied by Abdel-Kareem. (2014), using the experimental results. In addition, Moscoso *et al.* (2017) proposed numerical model should be able to trace the completely nonlinear response of these structures at service and ultimate loads. On the basis of the new innovative composite material is textile reinforced cementitious composite (TRCC), nine readymix repair mortars plates were presented by Daskiran *et al.* (2016).

Now a days, these innovative materials are increasingly being used in the manufacture of civil engenering, aerospace and aeronautical and in order to overcome the limitations of traditional methods, at recent years the novel and modified methods have been proposed for investigation of flexural and buckling behavior of the composite plates and concrete, for example (Ait Amar *et al.* 2014, Kolahchi and Bidgoli 2016, Arani and Kolahchi2016, Kolahchi *et al.* 2016a, b, 2017a, b, c, Bilouei *et al.* 2016, Zamanian *et al.* 2017, Hamid *et al.* 2016, Becheri *et al.* 2016, Hebali *et al.* 2016, Bouazza *et al.* 2016, Bousahla *et al.* 2016, Kolahchi and Cheraghbak 2017, Kolahchi 2017, Hajmohammad *et al.* 2017, 2018a, b, c, 2019, Zarei *et al.* 2017, Khetir *et al.* 2017, Amnieh *et al.* 2018, Golabchi *et al.* 2018, Ellali *et al.* 2018, Younsi *et al.* 2018, Bouhadra *et al.* 2018, Fakhar and Kolahchi 2018, Hosseini and Kolahchi 2018, Carvalho and Campilho 2017, Perrella *et al.* 2018, Abdelmalek *et al.* 2019, Berardi *et al.* 2019). Jassas *et al.* (2019) proposed a method vibration analysis of a concrete slab reinforced by SiO2 nanoparticles via Reddy theory. In addition, the frequency response of system is calculated based on the harmonic differential quadrature method (HDQM), finite element method (FEM) and Newmark method. In another work, Azmi *et al.* (2019) considered a visco-sinusoidal theory to investigate the dynamic response of sandwich plates subjected to blast load. The sandwich plate is composed of auxetic honeycombs core layer with negative Poisson's ratio integrated with nanocomposite at the top and bottom surfaces.

The behaviour of FRP concrete bonded joints under static and dynamic loadings, by developing a meso-scale finite element model using the concrete damage model in LS-DYNA studied by Li *et al.* (2015). Analysis of masonry structures strengthened with polymeric net reinforced cementitious matrix materials presented by D'Ambrisi *et al.* (2014) using experimental methodefor practical design applications and for assessing their seismic capacity. Experimental study of prestress losses of RC beams strengthened with prestress FRP presented by Huang *et al.* (2015). A total of 25 reinforced concrete (RC) beams strengthened with pre-tensioned carbon fiber reinforced polymer (CFRP) were conducted to investigate the prestress

*Corresponding author, Professor
E-mail: bouazza_mokhtar@yahoo.fr

http://www.techno-press.org/?journal=gae&subpage=7
ISSN: 2005-307X (Print), 2092-6219 (Online)

losses. Berardi *et al.* (2017) presented the creep behavior of GFRP laminates and their phases via experimental investigation and new analytical modeling. A creep test program was carried out in order to model the viscous behavior of the composites and their phases. A theoretical model proposed by Chen *et al.* (2018) used for studied the thin piezoelectric actuator attached to a graded half plane with an adhesive layer under an electrical loading. New approach by proposed by Berardi *et al.* (2018) capable to evaluate the stress migration from FRP to existing structural element, also accounting for the thin-walled sectional geometry of composite. in addition, capable to evaluate the influence of rheological properties of composite materials on the mechanical behavior of strengthened existing structures.

Earthquake analysis of nanofiber reinforced polymer-reinforced-concrete beams using hyperbolic shear deformation theory presented by Rad *et al.* (2017). A new composite reinforced method presented by Zhang et al (2018) namely self-compacting concrete filled circular CFRP-steel jacketing. Chen *et al.* (2018) presented the new theoretical model of a thin piezoelectric film bonded to a graded substrate under an in-plane electrical loading is established, in which the shear modulus of the graded substrate is assumed to vary exponentially in the thickness direction. Behavior of steel-concrete jacketed corrosion-damaged RC columns subjected to eccentric load studied by Hu *et al.* (2018). The strength and interfacial behavior of single lap joints with graded adherends subjected to uniaxial tensile loading are investigated by Chen *et al.* (2019).

The work presents a methodology for obtaining an analytical solution for the evaluation of interfacial shear and normal stresses of bonded composite plates under thermal effect. The proposed analytical approach is applied to the solution of simply supported beams strengthened with externally bonded composite plates $[\pm\theta_n/90_m]_S$ subjected to uniformly distributed loads and two symmetric point loads. Verification of the analytical solution is made through an example, where computed results were compared with other analytical approaches found in the specialized literature. Thereafter, a parametric study was carried out by varying other properties such as number of plies, fiber orientation, plate length, laminate thickness and adhesive layer thickness for different temperature increments. The work presents an interesting contribution for preliminary design purposes before considering debonding failures.

2. Mathematical model

The derivation of the new solution below is described in terms of adherends 1 and 2 (Fig. 1), where adherend 1 is the beam and adherend 2 is the soffit plate. Adherend 2 can be either steel or FRP but not limited to these two. The following assumptions were made in the analytical study:

1. All materials considered are linear elastic.
2. The beam is simply supported and shallow, that is, plane sections remain plane in bending.
3. No slip is allowed in the interface of the bond (i.e., there is a perfect bond at the adhesive steel or FRP plate interface).

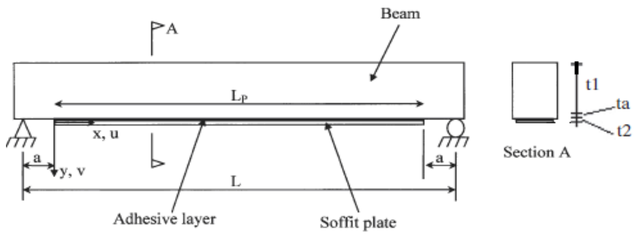

Fig. 1 Soffit-plated beam

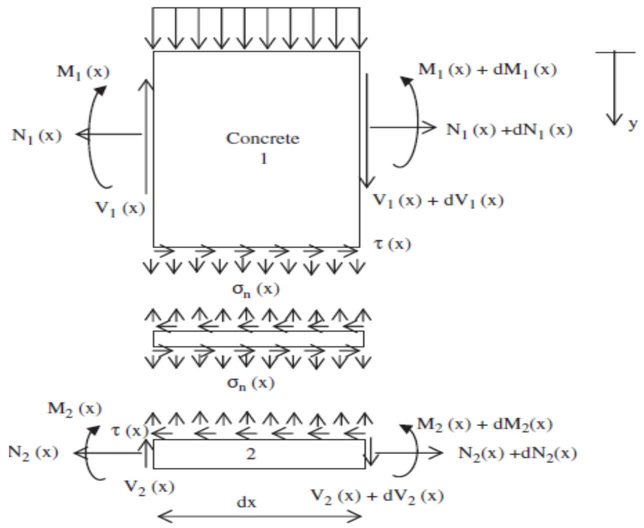

Fig. 2 Differential segment of a soffit-plated beam

4. Deformations of adherends 1 and 2 are due to bending moments and axial forces.
5. The shear stress analysis assumes that the curvatures in the beam and plate are equal (since this allows the shear stress and peel stress equations to be uncoupled). However, this assumption is not made in the peel stress solution. This assumption is used in several works e.g., Smith and Teng (2001), Tounsi (2006) and Stratford and Cadei (2004).

2.1 Adhesive shear stress: governing differential equation

A differential segment of a plated beam is shown in Fig. 2, where the interfacial shear and normal stresses are denoted by $\tau(x)$ and $\sigma(x)$, respectively. Fig. 2 also shows the positive sign convention for the bending moment, shear force, axial force and applied loading. The strains at the base of adherend 1 and the top of adherend 2, considering all three components of axial, bending and shear deformations, are given as

$$\varepsilon_1(x) = \frac{du_1(x)}{dx} = \frac{y_1}{E_1 I_1} M_1(x) - \frac{1}{E_1 A_1} N_1(x) + \alpha_1 \Delta T \quad (1)$$

where α_1 the thermal expansion coefficient, ΔT the temperature change, E_1 is the elastic modulus, $A_1$the cross-sectional area, $M_1$the bending moment, N_1 the axial force and y_1 the distance from the bottom of adherend 1 to its centroid.

Since the composite laminate is an orthotropic material, its material properties vary from layer to layer. In current

study, the laminate theory is used to determine the stress and strain behaviours of the externally bonded composite plate in order to investigate the whole mechanical performance of the composite-strengthened structure.
The effective moduli of the composite laminate are varied by the orientation of the fibre directions and arrangements of the laminate patterns. The laminate theory is used to estimate the strain of the symmetrical composite plate (Herakovich 1998), i.e.,

$$\varepsilon_x^0 = A'_{11} N_x \frac{1}{b_2} \quad \text{and}\ k_x = D'_{11} M_x \frac{1}{b_2} \tag{2}$$

$[A']=[A]^{-1}$ is the inverse of the extensional matrix $[A]$; $[D']=[D]^{-1}$ is the inverse of the flexural matrix; b_2 is a width of FRP plate.

Using classical laminate theory (CLT), the strain at the top of the FRP plate 2 is given as

$$\varepsilon_2(x) = \varepsilon_x^0 - k_x \frac{t_2}{2} + \alpha_2 \Delta T \tag{3}$$

Substituting Eq. (2) in (3) gives the following equation

$$\varepsilon_2(x) = -\frac{D'_{11} t_2}{2 b_2} M_2(x) + \frac{A'_{11}}{b_2} N_2(x) + \alpha_2 \Delta T \tag{4}$$

where

$$M_x = M_2(x), \ N_x = N_2(x) \tag{5}$$

The first derivative of the interfacial shear stress is given by

$$\frac{d\tau(x)}{dx} = \frac{G_a}{t_a}\left[\varepsilon_2(x) - \varepsilon_1(x)\right] \tag{6}$$

where G_a and t_a is the shear modulus and thickness of the adhesive layer. Substitution of Eqs. (1) and (4) into Eq. (6) yields

$$\frac{d\tau(x)}{dx} = \frac{G_a}{t_a}\left[(\alpha_2 - \alpha_1)\Delta T - \frac{D'_{11} t_2}{2 b_2} M_2(x) + \frac{A'_{11}}{b_2} N_2(x) - \frac{y_1}{E_1 I_1} M_1(x) + \frac{1}{E_1 A_1} N_1(x)\right] \tag{7}$$

Differentiating Eq. (7) with respect to x yields

$$\frac{d^2\tau(x)}{dx^2} = \frac{G_a}{t_a}\left(-\frac{D'_{11} t_2}{2 b_2}\frac{dM_2(x)}{dx} + \frac{A'_{11}}{b_2}\frac{dN_2(x)}{dx} - \frac{y_1}{E_1 I_1}\frac{dM_1(x)}{dx} + \frac{1}{E_1 A_1}\frac{dN_1(x)}{dx}\right) \tag{8}$$

The equilibrium of the differential segment dx shown in Fig. 2 gives the force equilibrium in the x direction for each adherent as

$$\frac{dN_1(x)}{dx} = \frac{dN_2(x)}{dx} = b_2 \tau(x) \tag{9}$$

where

$$N_1(x) = N_2(x) = N(x) = b_2 \int_0^x \tau(x) dx \tag{10}$$

and the moment equilibrium of the differential segment of the plated beam in Fig. 2 gives as

$$M_T(x) = M_1(x) + M_2(x) + N(x)\left(y_1 + \frac{t_2}{2} + t_a\right) \tag{11}$$

where, $M_T(x)$ is the total applied moment.

Assuming equal curvature in the beam and the FRP plate, the relationship between the moments in the two adherends can be expressed as

$$M_1(x) = R M_2(x) \tag{12}$$

with

$$R = \frac{D'_{11} E_1 I_1}{b_2} \tag{13}$$

The bending moment in each adherend, expressed as a function of the total applied moment and the interfacial shear stress, is given as

$$M_1(x) = \frac{R}{R+1}\left[M_T(x) - b_2 \int_0^x \tau(x)\left(y_1 + \frac{t_2}{2} + t_a\right) dx\right] \tag{14}$$

$$M_2(x) = \frac{1}{R+1}\left[M_T(x) - b_2 \int_0^x \tau(x)\left(y_1 + \frac{t_2}{2} + t_a\right) dx\right] \tag{15}$$

The first derivative of the bending moment in each adherend gives

$$\frac{dM_1(x)}{dx} = V_1(x) = \frac{R}{(R+1)}\left[V_T(x) - b_2 \tau(x)(y_1 + \frac{t_2}{2} + t_a)\right] \tag{16}$$

and

$$\frac{dM_2(x)}{dx} = V_2(x) = \frac{1}{(R+1)}\left[V_T(x) - b_2 \tau(x)(y_1 + \frac{t_2}{2} + t_a)\right] \tag{17}$$

Substitution of Eqs. (15), (16) and (10) into Eq. (8) yield the following governing differential equation for the interfacial shear stress

$$\frac{d^2\tau(x)}{dx^2} - \frac{G_a b_2}{t_a}\left(\frac{\left(y_1 + \frac{t_2}{2}\right)\left(y_1 + \frac{t_2}{2} + t_a\right)}{D'_{11} E_1 I_1 + b_2} b_2 D'_{11} + A'_{11} + \frac{b_2}{E_1 A_1}\right)\tau(x) + \frac{G_a}{t_a}\left(\frac{y_1 + \frac{t_2}{2}}{D'_{11} E_1 I_1 + b_2} D'_{11}\right) V_T(x) = 0 \tag{18}$$

The following general answer is considered for the second-order differential in Eq. (1)

$$\tau(x) = B_1 \cosh(\lambda x) + B_2 \sin h(\lambda x) + m_1 V_T(x) \tag{19}$$

where

$$\lambda^2 = \frac{G_a}{t_a}\left(\frac{(y_1 + \frac{t_2}{2})(y_1 + \frac{t_2}{2} + t_a)}{D'_{11} E_1 I_1 + b_2} b_2 D'_{11} + A'_{11} + \frac{b_2}{E_1 A_1}\right) \tag{20}$$

and

$$m_1 = \frac{G_a}{t_a}\frac{1}{\lambda^2}\left(\frac{\left(y_1 + \frac{t_2}{2}\right) D'_{11}}{D'_{11} E_1 I_1 + b_2}\right) \tag{21}$$

B_1 and B_2 are constant coefficients determined from the boundary conditions.

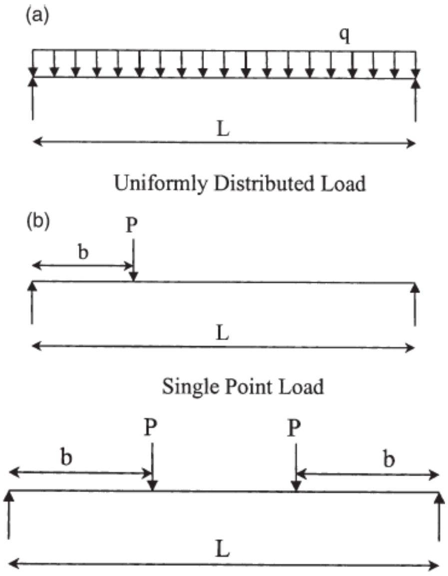

Fig. 3 Load cases

Note that the particular solution in Eq. (19) (i.e., $m_1 V_T(x)$) is valid only for the load distributions that result in $d2V_T(x)/d^2_x$=0, for example, when $V_T(x)$ is a constant or linear function. For the case when $V_T(x)$ is a function with a degree higher than one (e.g., quadratic, cubic, etc.), another appropriate particular solution shall be sought.

Having derived the general solutions for the interfacial shear and normal stresses, three load cases are now considered. A simply supported beam is investigated which is subjected to a uniformly distributed load and an arbitrarily positioned single point load, a as shown in Fig. 3.

Note that for the simplicity of the analysis, the shear deformation effects in both the RC beam and the FRP plate have been neglected in this paper. Substituting the appropriate expression for the shear force into Eq. (19) for the case of a simply supported beam subjected to a uniformly distributed load, the general answer for the interfacial shear stress is described by Smith and Teng 2001 as

$$\tau(x) = \left[\frac{m_2 a}{2}(L-a) - m_1\right]\frac{qe^{-\lambda x}}{\lambda} + m_{1.}q\left(\frac{L}{2} - a - x\right) \qquad 0 \le x \le L_p \tag{22}$$

where q is the uniformly distributed load and x, a, L and L_p are defined in Fig. 1, and the parameter m_2 is given as follows

$$m_2 = \frac{G_a y_1}{t_a E_1 I_1} \tag{23}$$

2.2 Adhesive peel-off stress: governing differential equation

The normal stress in the adhesive can be expressed as follows

$$\sigma(x) = \frac{E_a}{t_a}[v_2(x) - v_1(x)] \tag{24}$$

where $v_1(x)$ and $v_2(x)$ are the vertical displacements of adherend 1 and 2, respectively.

The equilibrium of adherends 1 and 2, neglecting second-order terms, leads to the following relationships.

Adherend 1

$$\frac{d^2 v_1(x)}{dx^2} = -\frac{1}{E_1 I_1} M_1(x) \tag{25}$$

$$\frac{dM_1(x)}{dx} = V_1(x) - b_2 y_1 \tau(x) \tag{26}$$

and

$$\frac{dV_1(x)}{dx} = -b_2\sigma(x) - q \tag{27}$$

Adherend 2

$$\frac{d^2 v_2(x)}{dx^2} = -\frac{D'_{11}}{b_2} M_2(x) \tag{28}$$

$$\frac{dM_2(x)}{dx} = V_2(x) - b_2\frac{t_2}{2}\tau(x) \tag{29}$$

and

$$\frac{dV_2(x)}{dx} = b_2\sigma(x) \tag{30}$$

Based on the above equilibrium equations, the governing differential equations for the deflection of adherends 1 and 2, expressed in terms of the interfacial shear and normal stresses, are given as follows

Adherend 1

$$\frac{d^4 v_1(x)}{dx^4} = \frac{1}{E_1 I_1} b_2\sigma(x) + \frac{1}{E_1 I_1} q + \frac{1}{E_1 I_1} b_2 y_1 \frac{d\tau(x)}{dx} \tag{31}$$

Adherend 2

$$\frac{d^4 v_2(x)}{dx^4} = -D'_{11}\sigma(x) + D'_{11}\frac{t_2}{2}\frac{d\tau(x)}{dx} \tag{32}$$

Substitution of Eqs. (31) and (32) into the fourth derivation of the interfacial normal stress obtainable from Eq. (24) gives the following governing differential equation for the interfacial normal stress

$$\frac{d^4\sigma(x)}{dx^4} + \frac{E_a}{t_a}\left(D'_{11} + \frac{b_2}{E_1 I_1}\right)\sigma(x) - \frac{E_a}{t_a}\left(D'_{11}\frac{t_2}{2} - \frac{y_1 b_2}{E_1 I_1}\right)\frac{d\tau(x)}{dx} + \frac{qE_a}{t_a E_1 I_1} = 0 \tag{33}$$

The general solution of differential equation is

$$\sigma(x) = e^{-\beta x}[C_1\cos(\beta x) + C_2\sin(\beta x)] - n_1\frac{d\tau(x)}{dx} - n_2 q \tag{34}$$

where

$$\beta = \sqrt[4]{\frac{E_a}{4t_a}\left(D'_{11} + \frac{b_2}{E_1 I_1}\right)} \tag{35}$$

$$n_1 = \left(\frac{y_1 b_2 - D'_{11}E_1 I_1\frac{t_2}{2}}{D'_{11}E_1 I_1 + b_2}\right) \tag{36}$$

and

$$\mathrm{n}_2 = \frac{1}{\mathrm{D}'_{11}\mathrm{E}_1\mathrm{I}_1 + \mathrm{b}_2} \tag{37}$$

C_1 and C_2 are constant coefficients determined from the boundary conditions.

The general solution for the interfacial shear stress for two symmetric point loads as shown in Fig. 3

$a < b$:

$$\tau(x) = \begin{cases} B_9 \cosh(\lambda x) + B_{10} \sinh(\lambda x) + m_1 P, & 0 \le x \le (b-a) \\ B_{11} \cosh(\lambda x) + B_{12} \cosh(\lambda x), & (b-a) \le x \le \frac{L_P}{2} \end{cases} \tag{38}$$

The boundary conditions are

$$\begin{aligned} &\text{at } x = 0, && M_1(0) = M_T(0) = Pa \\ &\text{at } x = \frac{L_P}{2}, && \tau\left(\frac{L_P}{2}\right) = 0 \\ &\text{at } x = (b-a), && \tau(x) \text{ is continuous, i.e.,} \\ &\text{at } x = (b-a), && \frac{d\tau(x)}{dx} \text{ is continuous, i.e.,} \end{aligned} \tag{39}$$

$$\left.\frac{d\tau_1(x)}{dx}\right|_{x=b-a} = \left.\frac{d\tau_2(x)}{dx}\right|_{x=b-a}$$

$$a > b: \quad \tau(x) = B_{13} \cosh(\lambda x) + B_{14} \sinh(\lambda x) \tag{40}$$

$$\begin{aligned} &\text{at } x = 0, && M_1(0) = M_T(0) = Pb \\ &\text{at } x = L_P, && M_1(L_P) = M_T(L_P) = Pb \end{aligned} \tag{41}$$

The constants coefficients with the thermal effect are determined to be

$$\begin{aligned} B_9 &= \frac{m_2}{\lambda} Pa - m_1 P e^{-k} - \frac{G_a(\alpha_1 - \alpha_2)\Delta T}{t_a \lambda}, \\ B_{10} &= -\frac{m_2}{\lambda} Pa + \frac{G_a(\alpha_1 - \alpha_2)\Delta T}{t_a \lambda} \\ B_{11} &= \frac{m_2}{\lambda} Pa + m_1 P \sinh(k) - \frac{G_a(\alpha_1 - \alpha_2)\Delta T}{t_a \lambda}, \quad B_{12} = -B_{11} \\ B_{13} &= \frac{m_2}{\lambda} Pb - \frac{G_a(\alpha_1 - \alpha_2)\Delta T}{t_a \lambda}, \qquad B_{14} = -B_{13} \end{aligned} \tag{42}$$

where

$$k = \lambda(b-a) \tag{43}$$

3. Numerical results and discussion

An RC beam bonded with a CFRP soffit plate is analysed. The beam is simply supported and subjected to a central point load or a uniformly distributed load. A summary of the geometric and material properties is given in Table 1. The span of RC beam is L=3000 mm, the distance from the support to the end of the plate is a=300 mm, the UDL is 50 KN/m and mid-point load is 150 KN.

Table1 Geometric and material properties

Material	E_{11} (MPa)	E_{22} (MPa)	G_{12} (MPa)	ν_{12}	Width (mm)	Depth (mm)
CFRP plate	140000	10000	5000	0.28	b_2=200	t_2=4
GFRP plate	50000	10000	5000	0.28	b_2=200	t_2=4
RC beam	30000	30000	--	0.18	b_2=200	t_1=300
Adhesive layer	3000	3000	--	0.35	b_2=200	ta=4

Table 2 Comparison of peak interfacial stresses in plated RC beams under UDL, MPa

Theory	GFRP plated		CFRP plated	
	$\tau(x)$	$\sigma(x)$	$\tau(x)$	$\sigma(x)$
Solution-1[a]	2.001	1.425	2.776	1.668
Solution-2[a]	1.813	1.256	2.591	1.500
Roberts (1989)	1.945	1.386	2.604	1.567
Malek *et al.* (1998)	1.943	1.384	2.597	1.563
Smith and Teng (2001)	1.975	1.244	2.740	1.484
Solution-3[b]	2.002	1.249	2.778	1.495
Yang and Wu (2007)	1.955	1.227	2.684	1.472
Tounsi (2006)	1.042	1.366	1.475	1.606
Solution-4[c]	1.298	1.184	1.834	1.518
Solution-5[d]	1.955	1.299	2.712	1.660
Qiao and Chen (2008)	---	---	2.052	1.442
Present	1.97496	1.24429	2.7404	1.48395

[a]Roberts and Haji-Kazemi (1989), [b]Narayanamurthy *et al.* (2010), [c]Narayanamurthy *et al.* (2011), [d]Narayanamurthy (2016)

Table 3 Comparison of peak interfacial stresses in plated RC beams under mid-point load, MPa

Theory	GFRP plated		CFRP plated	
	τ(x)	σ(x)	τ(x)	σ(x)
Roberts 1989	2.179	1.553	2.925	1.761
Taljsten 1989	2.215	1.397	3.087	1.674
Malek *et al.* 1998	2.179	1.553	2.925	1.761
Smith and Teng2001	2.214	1.396	3.083	1.671
Solution-4[c]	2.242	1.400	3.119	1.679
Solution-5[d]	2.182	1.465	3.041	1.885
Present	2.21414	1.39642	3.08297	1.67136

[c]Narayanamurthy *et al.* (2011), [d]Narayanamurthy (2016)

3.1 Comparison studies

In this section, various numerical examples are presented and discussed for verifying the accuracy and efficiency of the present method in predicting the interfacial shear and normal stresses RC beam bonded with a glass-fibre-reinforced plastic (GFRP) or CFRP soffit plate.

In both examples, the beams are simply supported and subjected to a uniformly distributed load. Table2 and 3, show the comparison of the interfacial shear and normal stresses from the closed form solutions of Roberts and Haji-Kazemi (solution-1 and solution-2) (1989), Roberts (1989), Malek *et al.* (1998), Smith and Teng (2001), Narayanamurthy *et al.* (2010), Yang and Wu (2007), Tounsi (2006), Narayanamurthy *et al.* (2011), Narayanamurthy (2016), Qiao and Chen (2008).

The interface stress distributions obtained by the present study and other existing models are shown in Figs. 4-7 for the interface shear and normal stresses near the plate end of the plated beam under the UDL and subjected to a mid-

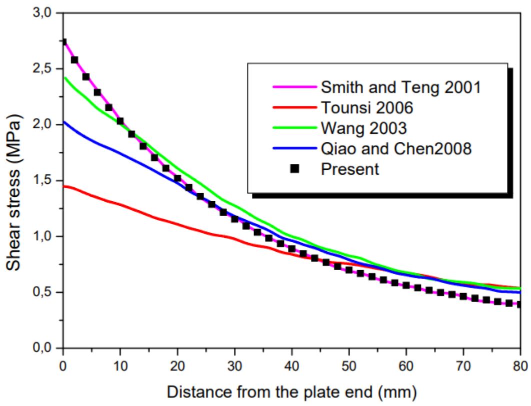

Fig. 4 Comparison of interfacial shear stresses for an RC beam with a bonded CFRP soffit plate subjected to a UDL

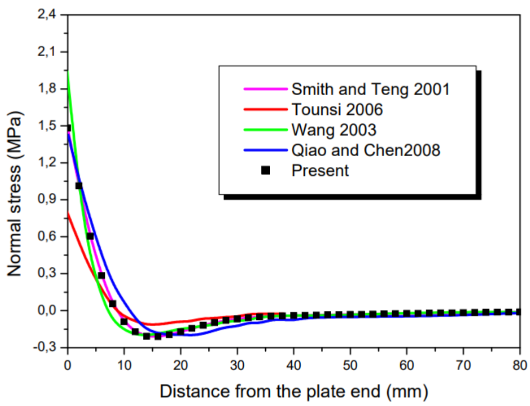

Fig. 5 Comparison of interfacial normal stresses for an RC beam with a bonded CFRP soffit plate subjected to a UDL

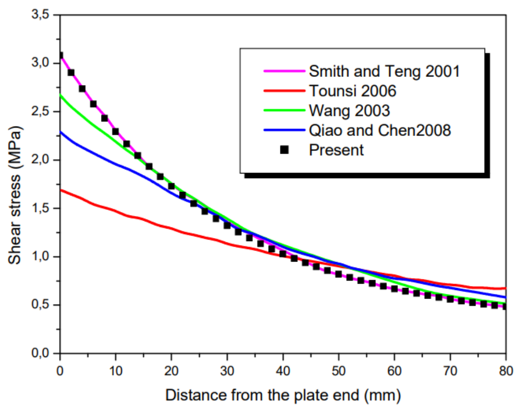

Fig. 6 Comparison of interfacial shear stresses for an RC beam with a bonded CFRP soffit plate subjected to a mid-point load

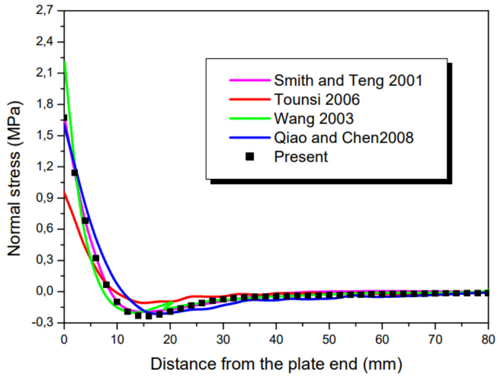

Fig. 7 Comparison of interfacial normal stresses for an RC beam with a bonded CFRP soffit plate subjected to a mid-point load

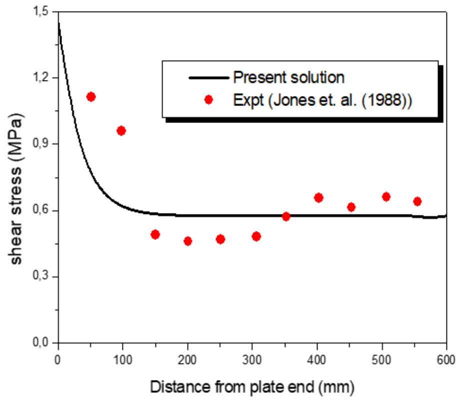

Fig. 8 Comparison of theoretical results with experimental results

point load cases, respectively. As demonstrated in Figs. 4-7, good agreements of the interface stresses among all the comparisons are reached at the large distance away from the plate end.

The predicted interfacial shear stress by the present theory has been compared to those of experimental results obtained by Jones *et al.* (1988). The geometry and materials properties of the strengthened beam are b1=155 mm, t_1=225 mm, L=2300 mm, E_1=31 GPa, G_1=13.14 GPa. The geometry and materials properties of the plate are b_2=125 mm, t_2=6 mm, L_p=2200 mm, E_2=200 GPa, G_1=76.92 GPa, for the adhesive layer, thickness t_a=1.5 mm, elastic modulus E_a=3 GPa, and shear moulus G_a=1.11 GPa. As it can be seen from Fig. 8 the predicted theoretical results are in general agreement with the 'test' results presented by Jones *et al.* (1988). The example RC beam bonded with a thin steel plate subjected to a four point bending with two transverse loads each of 30 kN.

3.2 Parametric studies

To better understand the behaviour of characteristics of interfacial stress distributions in these strengthened beams, the effects of a few parameters were investigated.

3.2.1 Effects of temperature

The same example plated beam is considered here to examine the interfacial stress distributions due to a temperature change. The temperature was assumed to a uniform temperature rise of 0°C, 50°C and 100°C. The coefficients of thermal expansion are as follows: $\alpha_1=10\times10^{-6}$°C^{-1} for the concrete and $\alpha_2=9\times10^{-6}$°C^{-1}for the CFRP-plate (Schmit (1998)). Fig. 9 show the stacking sequences used in the studied example.

The mechanical properties of material can be impacted

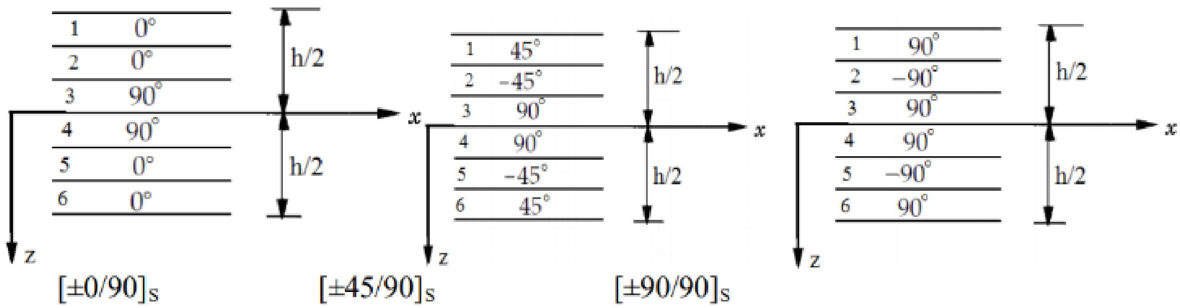

Fig. 9 Stacking sequences used in the studied example

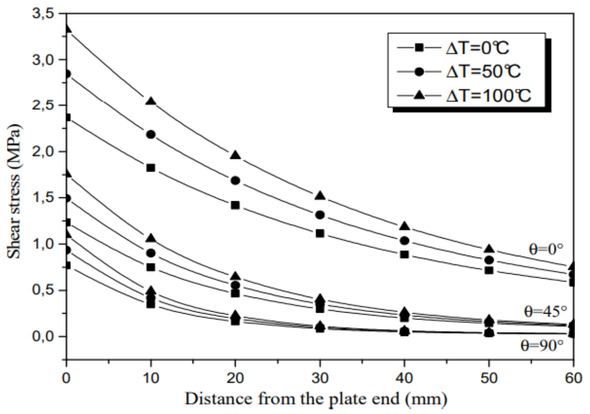

Fig. 10 Thermal effect on the interfacial shear stresses for an RC beam with a bonded composites laminates plate [±θ/90]s

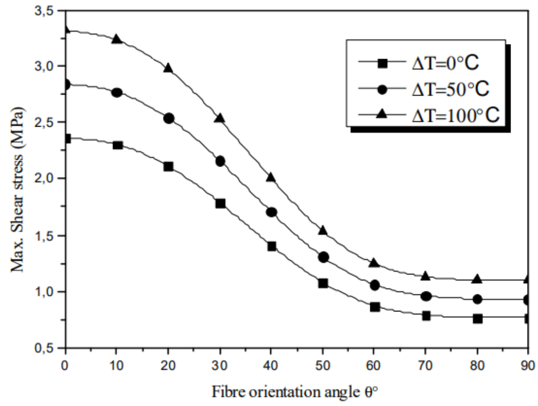

Fig. 12 Effect of the fibre orientation on the interfacial shear stresses for an RC beam with a bonded composites laminates plate [±θ/90]s under thermal effect

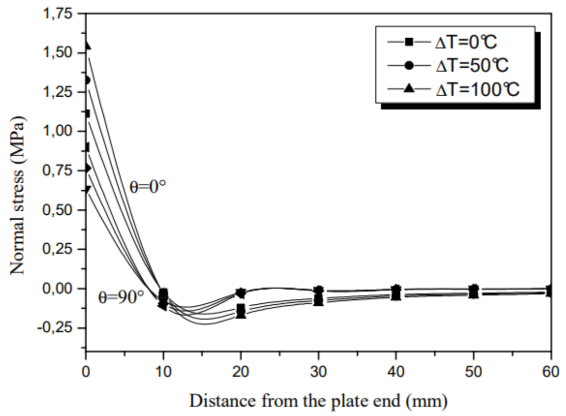

Fig. 11 Thermal effect on the interfacial normal stresses for an RC beam with a bonded composites laminates plate [±θ/90]s

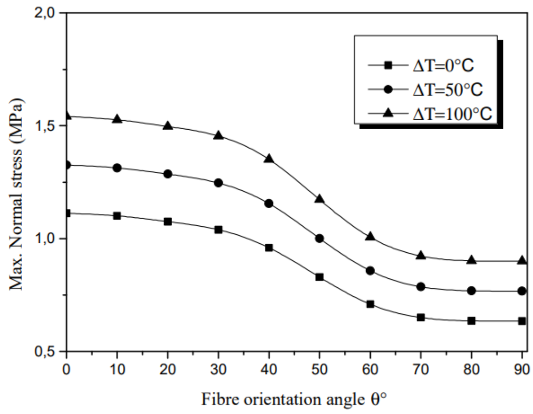

Fig. 13 Effect of the fibre orientation on the interfacial normal stresses for an RC beam with a bonded composites laminates plate [±θ/90]s under thermal effect

by temperature, which leads to variation of behavoir characteristics of the structures. Specifically, the bending characteristics of the beam can be affected by thermal effects in two forms, which consist of thermal expansion deformation and variations of material properties (elastic modulus) with temperature. Figs. 10 and 11, illustrates the effects of temperature on the interfacial shear and normal stresses near the plate end for the example RC beam bonded with a CFRP plate. The outer layers CFRP plate the stacking sequences [±θ/90]S, with θ = 0, 45 and 90. It is found that the increase of temperature leads to the increasing of the interfacial shear and normal.

3.2.2 Effect of fibre orientation in the outer plies

In Figs. 12 and 13 the maximum interfacial shear stresses and the maximum normal stress, respectively are plotted as a function of the fibre angle of outer layers,θ, for there values of temperatures (ΔT=0,50 and 100). This study that the fibers orientation [±θ/90]s .It has been observed that the maximum interfacial shear and maximum normal stresses reduces monotonically with increased fibre angle, whatever the temperature expansion.

3.2.3 Effect of number of 90 layers in the central sublaminate

The interfacial stresses as a function of a varying

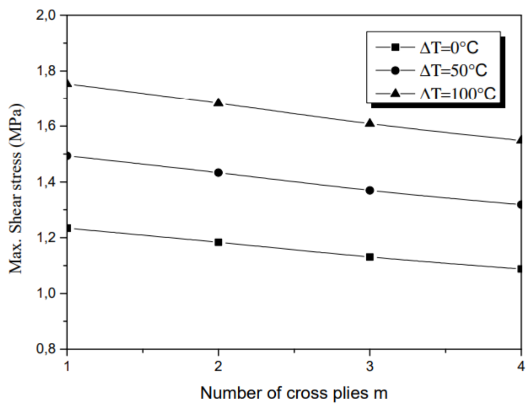

Fig. 14 Effect of number of 90 plies for $[\pm 45/90_m]_S$ on edge shear stresses in RC beam with a bonded composites laminates plate under thermal effect

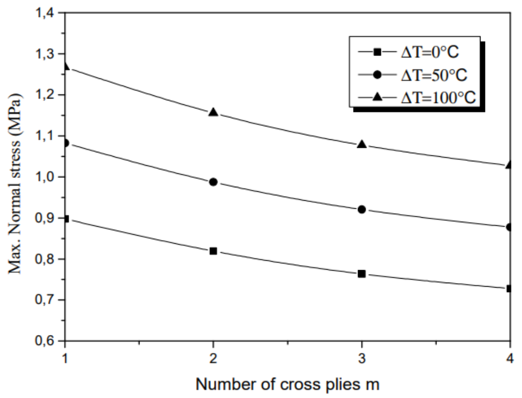

Fig. 15 Effect of number of 90 plies for $[\pm 45/90_m]_S$ on edge normal stresses in RC beam with a bonded composites laminates plate under thermal effect

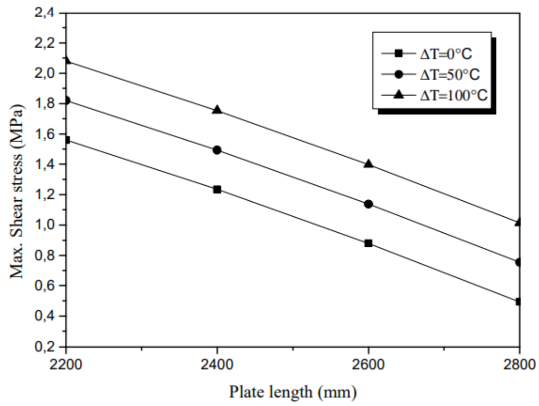

Fig. 16 Effect of plate length on interfacial shear stresses in RC beam with a bonded composites laminates plate $[\pm 45/90]_S$ under thermal effect

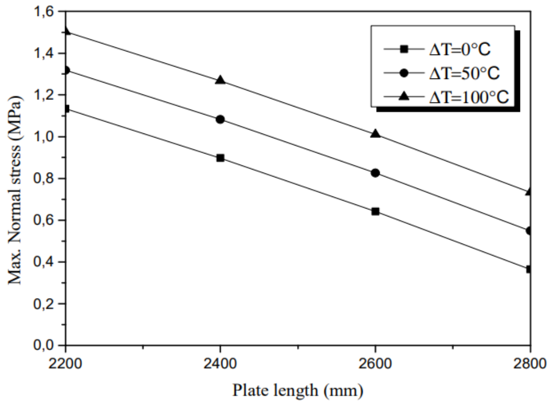

Fig. 17 Effect of plate length on interfacial normal stresses in RC beam with a bonded composites laminates plate $[\pm 45/90]_S$ under thermal effect

number of 90° layers and a constant number of 45° layers for $[\pm 45/90_m]_S$ laminate with three temperature is shown in Figs. 14 and 15. The interfacial stresses are more in case of laminates with a larger number of 90 plies. This is due to the stiffness reduction is more in the case of laminates with a greater number of central 90 plies.

3.2.4 Effect on plate length of the strengthened beam region

Figs. 16 and 17 show that the with the increase of the length of the strengthened beam region Lp for three type of temperature. It is seen that, as the plate terminates further away from the supports, the interfacial stresses increase significantly. This result reveals that in any case of strengthening, including cases where retrofitting is required in a limited zone of maximum bending moments at mid span, it is recommended to extend the strengthening strip as close as possible to the support lines.

3.2.5 Effect of the laminate thickness

The thickness of the laminate plate is an important design variable in practice. Peak shear and normal stress for various thickness of FRP angle-ply composites laminates plate appear in Figs. 18 and 19 it is shown that the level and concentration of interfacial stress are influenced considerably by the thickness of FRP plate. The interfacial stresses increase as the thickness of FRP plate increases.

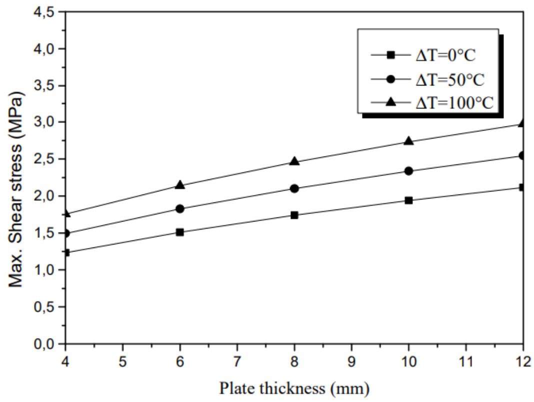

Fig. 18 Effect of the laminate plate thickness on interfacial shear stresses in RC beam with a bonded composites laminates plate $[\pm 45/90]_S$ under thermal effect

3.2.6 Effect of adhesive layer thickness

Figs. 20 and 21 show the effect of the thickness of the adhesive layer on interfacial stress. It is seen that increasing the thickness of the adhesive layer leads to significant reduction in peak interfacial stress. Thus using thick

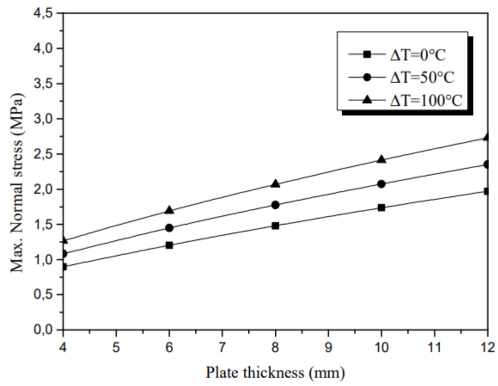

Fig. 19 Effect of the laminate plate thickness on interfacial normal stresses in RC beam with a bonded composites laminates plate $[\pm 45/90]_S$ under thermal effect

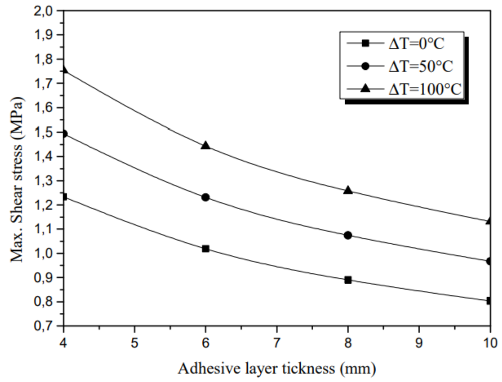

Fig. 20 Effect of adhesive layer thickness on interfacial shear stresses in RC beam with a bonded composites laminates plate $[\pm 45/90]_S$ under thermal effect

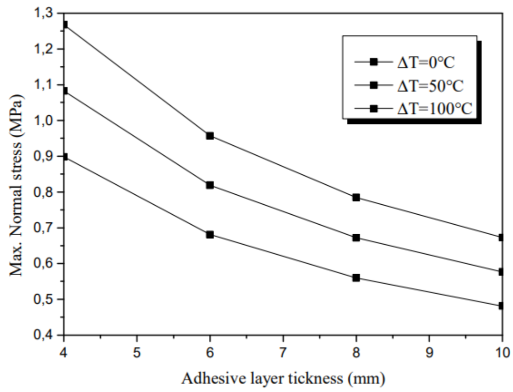

Fig. 21 Effect of adhesive layer thickness on interfacial normal stresses in RC beam with a bonded composites laminates plate $[\pm 45/90]_S$ under thermal effect

adhesive layer, especially in the vicinity of the edge, is recommended.

4. Conclusions

A closed-form rigorous solution for interfacial stress in simply supported beams strengthened with bonded prestressed FRP angle-ply composites laminates plate and subjected to mid-point load or uniformly distributed load and thermal environment are presented in this paper. Predictions of such stresses are prerequisite for designing against debonding failures of the FRP plate from the RC beam. Comparison studies are performed to verify the validity of present results. The effects of temperature and variations of fibre orientation in the outer plies, number of 90 layers in the central sublaminate, plate length of the strengthened beam region, laminate thickness, and adhesive layer thickness on the interfacial shear and normal stresses are investigated and discussed. On the basis of the present results the following conclusions can be drawn:

- The results obtained by present model are compared with those found in the literature. It can be concluded that the present model is not only accurate but also efficient in predicting the interfacial stresses.

- The interfacial stresses are influenced by the geometry parameters such as thickness of the adhesive layer and FRP plate in range of the different degrees. It is shown that the edge stresses and levels increase obviously with the increase of the thickness of the FRP plate. However, it is seen that increasing the thickness of the adhesive layer leads to significant reduction in the peak interfacial stresses.

- It is observed that the interfacial stresses decreases with increasing number of layers at 90° for a fixed number of layers at ±45 °. On the other hand, the interfacial stresses are also reduced with decreasing temperature.

- It has been shown that, provided the material properties are not affected by temperature variations, a temperature rise increases the interfacial shear stresses and interfacial normal stresses while a temperature reduction decreases the interfacial stresses; the latter can have serious implications for the safety of the strengthened structure.

- Stiffness's of the FRP $[\pm\theta/90]_S$ angle-ply laminates largely depend on the fibre orientation angle θ of the outer layers. However, the maximum interfacial stresses decrease with increasing the fibre orientation angle of the outer layers of angle-ply composites laminates.

- The use of the FRP plate with different fibre orientations results changes the stiffeness of the composite plate. Having high-strength fibres aligned in the beam direction would maximize the thickness of the plate, while having the fibers aligned perpendicularly to the beam axis would greatly reduce the interfacial shear and normal stresses. The maximum adhesive stresses increase with increasing alignment of all high-strength fibers in the composite plate in beam's longitudinal direction x.

- Finally, we deduce that the building structures using FRP composites can increase the life of these structures and participate in the cleanliness of the environment and reduce pollution.

Due to the interesting features of the present model , the present findings will be a useful benchmark for evaluating the reliable of other future models the interfacial stresses in plated beams .

Acknowledgments

The authors thank the referees for their valuable comments.

References

Abdel-Kareem, A.H. (2014), "Shear strengthening of reinforced concrete beams with rectangular web openings by FRP composites", *Adv. Concrete Construct.*, **2**(4),281-300. http://dx.doi.org/10.12989/acc.2014.2.4.281/.

Abdelmalek, A., Bouazza, M., Zidour, M. and Benseddiq, N. (2019), "Hygrothermal effects on the free vibration behavior of composite plate using nth-order shear deformation theory: A micromechanical approach", *Iran J. Sci. Technol. Trans. Mech. Eng.*, **43**(1), 61-73. https://doi.org/10.1007/s40997-017-0140-y.

Ait Amar. M, Abdelaziz, H.H. and Tounsi. A. (2014), "An efficient and simple refined theory for buckling and free vibration of exponentially graded sandwich plates under various boundary conditions", *J. Sandw. Struct. Mater.*, **16**(3), 293-318. https://doi.org/10.1177%2F1099636214526852.

Amnieh, H.B., Zamzam, M.S. and Kolahchi, R. (2018), "Dynamic analysis of non homogeneous concrete blocks mixed by SiO2 nanoparticles subjected to blast load experimentally and theoretically", *Constr. Build. Mater.*, **174**, 633-644. https://doi.org/10.1016/j.conbuildmat.2018.04.140.

Arani, A.J. and Kolahchi, R. (2016), "Buckling analysis of embedded concrete columns armed with carbon nanotubes", *Comput. Concrete*, **17**(5), 567-578. http://dx.doi.org/10.12989/cac.2016.17.5.567.

Azmi, M., Kolahchi, R. and Bidgoli, M.R. (2019), "Dynamic analysis of concrete column reinforced with Sio2 nanoparticles subjected to blast load", *Adv. Concrete Construct.*, **7**(1), 51-63. https://doi.org/10.12989/acc.2019.7.1.051.

Becheri, T., Amara, K., Bouazza, M. and Benseddiq, N. (2016), "Buckling of symmetrically laminated plates using nth-order shear deformation theory with curvature effects", *Steel Compos. Struct.*, **21**(6), 1347-1368. https://doi.org/10.12989/scs.2016.21.6.1347.

Berardi, V.P., Perrella, M., Feo, L. and Cricrì, G. (2017), "Creep behavior of GFRP laminates and their phases: Experimental investigation and analytical modeling", *Compos. B Eng.*, **122**, 136-144. https://doi.org/10.1016/j.compositesb.2017.04.015.

Berardi, V.P., Feo, L., Mancusi, G. and De Piano, M. (2018), "Influence of reinforcement viscous properties on reliability of existing structures strengthened with externally bonded composites", *Compos. Struct.*, **200**, 532-539. https://doi.org/10.1016/j.compstruct.2018.05.111.

Berardi, V.P., Perrella, M. and Cricrì, G. (2019), "Cohesive fracture in composite systems: experimental setup and first results", *Frattura ed Integrità Strutturale*, **48**, 222-229. https://doi.org/10.3221/IGF-ESIS.48.23.

Bilouei, B.S., Kolahchi, R. and Bidgoli, M.R. (2016), "Buckling of concrete columns retrofitted with Nano-Fiber Reinforced Polymer (NFRP)", *Comput. Concrete*, **18**(5), 1053-1063. https://doi.org/10.12989/cac.2016.18.5.1053.

Bouazza, M., Lairedj, A., Benseddiq, N. and Khalki, S. (2016), "A refined hyperbolic shear deformation theory for thermal buckling analysis of cross-ply laminated plates", *Mech. Res. Commun.*, **73**, 117-126. https://doi.org/10.1016/j.mechrescom.2016.02.015.

Bouhadra, A., Tounsi, A., Bousahla, A.A., Benyoucef, S. and Mahmoud, S.R. (2018), "Improved HSDT accounting for effect of thickness stretching in advanced composite plates", *Struct. Eng. Mech.*, **66**(1), 61-73. https://doi.org/10.12989/sem.2018.66.1.061.

Bousahla, A.A., Benyoucef, S. Tounsi, A. and Mahmoud, S.R. (2016), "On thermal stability of plates with functionally graded coefficient of thermal expansion", *Struct. Eng. Mech.*, **60**(2), 313-335. https://doi.org/10.12989/sem.2016.60.2.313.

Carvalho, U.T.F. and Campilho, R.D.S.G. (2017), "Validation of pure tensile and shear cohesive laws obtained by the direct method with single-lap joints", *Int. J. Adhes. Adhes.*, **77**, 41-50. https://doi.org/10.1016/j.ijadhadh.2017.04.002.

Chen, P., Chen, S., Guo, W. and Gao, F. (2018), "The interface behavior of a thin piezoelectric film bonded to a graded substrate", *Mech. Mater.*, **127**, 26-38. https://doi.org/10.1016/j.mechmat.2018.08.009.

Chen, P., Guo, W., Zhao, Y., Li, E., Yang, Y. and Liu, H. (2019), "Numerical analysis of the strength and interfacial properties of adhesive joints with graded adherends", *Int. J. Adhes. Adhes.*, **90**, 88-96. https://doi.org/10.1016/j.ijadhadh.2019.02.003.

Chen, P., Peng, J., Liu, H., Gao, F. and Guo, W. (2018), "The electromechanical behavior of a piezoelectric actuator bonded to a graded substrate including an adhesive layer", *Mech. Mater.*, **123**, 77-87. https://doi.org/10.1016/j.mechmat.2018.05.002.

Civalek, O. and Yavas, A. (2008), "Discrete singular convolution for buckling analyses of plates and columns", *Struct. Eng. Mech.*, **29**(3)., 279-288. https://doi.org/10.12989/sem.2008.29.3.279.

D'Ambrisi, A., Mezzi, M., Feo, L. and Berardi, V.P. (2014) "Analysis of masonry structures strengthened with polymeric net reinforced cementitious matrix materials", *Compos. Struct.*, **113**, 264-271. https://doi.org/10.1016/j.compstruct.2014.03.032.

Daskiran, E.G., Daskiran, M.M. and Gencoglu, M. (2016), "Development of fine grained concretes for textile reinforced cementitious composites", *Comput. Concrete*, **18** (2), 297-295. http://dx.doi.org/10.12989/cac.2016.18.2.279.

Ellali, M., Amara, K., Bouazza, M. and Bourada, F. (2018), "The buckling of piezoelectric plates on Pasternak elastic foundation using higher-order shear deformation plate theories", *Smart Struct. Syst.*, **21**(1), 113-122. https://doi.org/10.12989/sss.2018.21.1.113.

Fakhar, A. and Kolahchi, R. (2018), "Dynamic buckling of magnetorheological fluid integrated by viscopiezo-GPL reinforced plates", *Int. J. Mech. Sci.*, **144**, 788-799. https://doi.org/10.1016/j.ijmecsci.2018.06.036.

Forquin, P. and Hild, F. (2008), "Dynamic fragmentation of an ultra-high strength concrete during edge-on impact tests", *J. Eng. Mech.*, **134**(4), 302-315. https://doi.org/10.1061/(ASCE)0733-9399(2008)134:4(302).

Fragiacomo, M. (2005), "A finite element model for long-term analysis of timber-concrete composite beams", *Struct. Eng. Mech.*, **20**(2), 173-189. https://doi.org/10.12989/sem.2005.20.2.173.

Golabchi, H., Kolahchi, R. and Bidgoli, M.R. (2018), "Vibration and instability analysis of pipes reinforced by SiO2 nanoparticles considering agglomeration effects", *Comput. Concrete*, **21**(4), 431-440. https://doi.org/10.12989/cac.2018.21.4.431.

Hajmohammad, M.H., Farrokhian, A. and Kolahchi, R. (2018a), "Smart control and vibration of viscoelastic actuator-multiphase nanocomposite conical shells-sensor considering hygrothermal load based on layerwise theory", *Aerosp. Sci. Technol.*, **78**, 260-270. https://doi.org/10.1016/j.ast.2018.04.030.

Hajmohammad, M.H., Kolahchi, R., Zarei, M.S. and Maleki, M. (2018c), "Earthquake induced dynamic deflection of submerged viscoelastic cylindrical shell reinforced by agglomerated CNTs considering thermal and moisture effects", *Compos. Struct.*, **187**, 498-508. https://doi.org/10.1016/j.compstruct.2017.12.004.

Hajmohammad, M.H., Maleki, M. and Kolahchi, R. (2018b), "Seismic response of underwater concrete pipes conveying fluid covered with nano-fiber reinforced polymer layer", *Soil Dyn. Earthq. Eng.*, **110**, 18-27. https://doi.org/10.1016/j.soildyn.2018.04.002.

Hajmohammad, M.H., Zarei, M.S., Nouri, A. and Kolahchi, R. (2017), "Dynamic buckling of sensor/functionally graded-carbon nanotube-reinforced laminated plates/actuator based on sinusoidalvisco-piezoelasticity theories", *J. Sandw. Struct.*

Mater., 1099636217720373. https://doi.org/10.1177%2F1099636217720373.

Hajmohammada, M.H., Kolahchi, R., Sharif Zarei, M., Nouri AH (2019), "Dynamic response of auxetic honeycomb plates integrated with agglomerated CNT-reinforced face sheets subjected to blast load based on visco-sinusoidal theory", *Int. J. Mech. Sci*., **153** 391-401. https://doi.org/10.1016/j.ijmecsci.2019.02.008.

Hebali, H., Bakora, A., Tounsi, A. and Kaci, A. (2016), "A novel four variable refined plate theory for bending, buckling, and vibration of functionally graded plates", *Steel Compos. Struct*., **22**(3), 473-495. https://doi.org/10.12989/scs.2016.22.3.473.

Herakovich, C.T. (1998), *Mechanics of Fibrous Composites*, Wiley, U.S.A.

Hoque, M., Rattanawangcharoen, N., Shah, A.H. and Desai, Y.M. (2007), "3D nonlinear mixed finite-element analysis of RC beams and plates with and without FRP reinforcement", *Comput. Concrete*, **4**(2), 135-156. http://dx.doi.org/10.12989/cac.2007.4.2.135.

Hosseini, H. and Kolahchi, R. (2018), "Seismic response of functionally graded-carbon nanotubesreinforced submerged viscoelastic cylindrical shell in hygrothermal environment", *Phys. E Low-Dimens. Syst. Nanostruct*., **102**, 101-109. https://doi.org/10.1016/j.physe.2018.04.037.

Hu, J., Liang, H. and Lu, Y. (2018), "Behavior of steel-concrete jacketed corrosion-damaged RC columns subjected to eccentric load", *Steel Compos. Struct*., **29**(6), 689-701. https://doi.org/10.12989/scs.2018.29.6.689.

Huang, J., Huang, P.X. and Zheng, X. (2015), "Experimental study of prestress losses of RC beams strengthened with prestress FRP", *J. Build. Struct*., **36**(1), 85-91.

Jassas, M.R., Bidgoli, M.R. and Kolahchi R.(2019), "Forced vibration analysis of concrete slabs reinforced by agglomerated SiO2 nanoparticles based on numerical methods", *Construct. Build. Mater*., **211**, 796-806. https://doi.org/10.1016/j.conbuildmat.2019.03.263.

Kara, I.K. and Dundar, C. (2012), "Prediction of deflection of high strength steel fiber reinforced concrete beams and columns", *Comput. Concrete*, **9**(2), 133-151. http://dx.doi.org/10.12989/cac.2012.9.2.133/

Khetir, H., Bouiadjra, M.B., Houari, M.S.A., Tounsi, A. and Mahmoud, S.R. (2017), "A new nonlocal trigonometric shear deformation theory for thermal buckling analysis of embedded nanosize FG plates", *Struct. Eng. Mech*., **64**(4), 391-402. https://doi.org/10.12989/sem.2017.64.4.391.

Kolahchi, R. (2017), "A comparative study on the bending, vibration and buckling of viscoelastic sandwich nano-plates based on different nonlocal theories using DC, HDQ and DQ methods", *Aerosp. Sci. Technol*., **66**, 235-248. https://doi.org/10.1016/j.ast.2017.03.016.

Kolahchi, R. and Bidgoli, A.M. (2016), "Size-dependent sinusoidal beam model for dynamic instability of single-walled carbon nanotubes", *Appl. Math. Mech*., **37**(2), 265-274. https://doi.org/10.1007/s10483-016-2030-8.

Kolahchi, R. and Cheraghbak, A. (2017), "Agglomeration effects on the dynamic buckling of viscoelastic microplates reinforced with SWCNTs using Bolotin method", *Nonlin. Dyn*., **90**(1), 479-492. https://doi.org/10.1007/s11071-017-3676-x.

Kolahchi, R., Hosseini, H. and Esmailpour, M. (2016a), "Differential cubature and quadrature-Bolotin methods for dynamic stability of embedded piezoelectric nanoplates based on visco-nonlocalpiezoelasticity theories", *Compos. Struct*., **157**, 174-186. https://doi.org/10.1016/j.compstruct.2016.08.032.

Kolahchi, R., Keshtegar, B. and Fakhar, M.H. (2017c), "Optimization of dynamic buckling for sandwich nanocomposite plates with sensor and actuator layer based on sinusoidal-visco-piezoelasticity theories using Grey Wolf algorithm", *J. Sandw. Struct. Mater*., 1099636217731071. https://doi.org/10.1177%2F1099636217731071.

Kolahchi, R., Safari, M. and Esmailpour, M. (2016b), "Dynamic stability analysis of temperature-dependent functionally graded CNT-reinforced visco-plates resting on orthotropic elastomeric medium", *Compos. Struct*., **150**, 255-265. https://doi.org/10.1016/j.compstruct.2016.05.023.

Kolahchi, R., Zarei, M.S., Hajmohammad, M.H. and Nouri, A. (2017b), "Wave propagation of embedded viscoelastic FG-CNT-reinforced sandwich plates integrated with sensor and actuator based on refined zigzag theory", *Int. J. Mech. Sci*., **130**, 534-545. https://doi.org/10.1016/j.ijmecsci.2017.06.039.

Kolahchi, R., Zarei, M.S., Hajmohammad, M.H. and Oskouei, A.N. (2017a), "Visco-nonlocal-refined Zigzag theories for dynamic buckling of laminated nanoplates using differential cubature-Bolotin methods", *Thin-Wall. Struct*., **113**, 162-169. https://doi.org/10.1016/j.tws.2017.01.016.

Madani, H., Hosseini, H. and Shokravi, M. (2016), "Differential cubature method for vibration analysis of embedded FG-CNT-reinforced piezoelectric cylindrical shells subjected to uniform and non-uniform temperature distributions", *Steel Compos. Struct*., **22**(4), 889-913. https://doi.org/10.12989/scs.2016.22.4.889.

Malek, A.M., Saadatmanesh, H. and Ehsani, M.R. (1998), "Prediction of failure load of RC beams strengthened with FRP plate due to stress concentration at the plate end", *ACI Struct. J*., **95**(1), 142-152.

Moscoso, A.M., Tamayo, J.L. and Morsch, I.B. (2017), "Numerical simulation of external pre-stressed steel-concrete composite beams", *Comput. Concrete*, **19**(2), 191-201. https://doi.org/10.12989/cac.2017.19.2.191.

Narayanamurthy, V., Chen, J.F. and Cairns, J. (2010), "A general analytical method for the analysis of in terfacial stresses in plated beams under arbitrary loading", *Adv. Struct. Eng*., **13**(5), 975-988. https://doi.org/10.1260%2F1369-4332.13.5.975.

Narayanamurthy, V., Chen, J.F. and Cairns, J. (2016), "Improved model for interfacial stresses accounting for the effect of shear deformation in plated beams", *Int. J. Adhes. Adhes*., **64**, 33-47. https://doi.org/10.1016/j.ijadhadh.2015.10.001.

Narayanamurthy, V., Chen, J.F., Cairns, J. and Ramaswamy, A. (2011), "Effect of shear deformationon interfacial stresses of plated beams subjected to arbitrary loading", *Int. J. Adhes*., *Adhes*., **31**(8), 862-874. https://doi.org/10.1016/j.ijadhadh.2011.08.007.

Oehlers, D.J., Nguyen, N.T., Ahmed, M. and Bradford, M.A. (1997), "Transverse and longitudinal partial interaction in composite bolted side-plated reinforced-concrete beams", *Struct. Eng. Mech*,, **5**(5), 553-563. https://doi.org/10.12989/sem.1997.5.5.553.

Perrella, M., Berardi, V.P. and Cricrì, G. (2018), "A novel methodology for shear cohesive law identification of bonded reinforcements", *Compos. Part B Eng*., **144**, 126-133. https://doi.org/10.1016/j.compositesb.2018.02.027.

Qiao, P. and Chen, F. (2008), "An improved adhesively bonded bi-material beam model for plated beams", *Eng. Struct*., **30**(7), 1949-1957. https://doi.org/10.1016/j.engstruct.2007.12.017.

Rad, S.S. and Bidgoli, MR (2017), "Earthquake analysis of NFRP-reinforced-concrete beams using hyperbolic shear deformation theory", *Earthq. Struct*., **13**(3), 241-253. https://doi.org/10.12989/eas.2017.13.3.241.

Roberts, T.M. (2001), "Approximate analysis of shear and normal stress concentrations in the adhesive layer of plated RC beams", *J. Struct. Eng*., **10**(2), 229-233

Roberts, T.M. and Hajikazemi, H. (1989), "Theoretical study of the behaviour of reinforced concrete beams strengthened by externally bonded steel plates", *Proc. Inst. Civ. Eng*., **87**(2), 39-55. https://doi.org/10.1680/iicep.1989.1452.

Schmit, K. (1998), *Fiberglass Reinforced Plastic (FRP) Piping Systems Designing Process / Facilities Piping Systems with FRP a Comparison to Traditional Metallic Materials*, Project Engineer Specialty Plastics, Inc., Baton Rouge, Los Angeles, California, U.S.A.

Siu, W.H. and Su, R.K.L. (2011), "Analysis of side-plated reinforced concrete beams with partial interaction", *Comput. Concrete*, **8**(1), 71-96. https://doi.org/10.12989/cac.2011.8.1.071.

Smith, S.T. and Teng, J.G. (2001), "Interfacial stresses in plated beams", *Eng. Struct.*, **23**(7), 857-871. https://doi.org/10.1016/S0141-0296(00)00090-0.

Taljsten, B. (1997), "Strengthening of beams by plate bonding", *J. Mater. Civ. Eng.*, **9**(4), 206-212. https://doi.org/10.1061/(ASCE)0899-1561(1997)9:4(206).

Teng, J.G., Chen, J.F., Smith, S.T. and Lam, L. (2001), "FRP strengthened RC structures", *Front. Phys*.

Tounsi, A. (2006), "Improved theoretical solution for interfacial stresses in concrete beams strengthened with FRP plate", *Int. J. Solids Struct.*, **43**(14-15), 4154-4174. https://doi.org/10.1016/j.ijsolstr.2005.03.074.

Younsi, A., Tounsi, A., Zaoui, F.Z., Bousahla, A.A. and Mahmoud, S.R. (2018), "Novel quasi-3D and 2D shear deformation theories for bending and free vibration analysis of FGM plates", *Geomech. Eng.*, **14**(6), 519-532. https://doi.org/10.12989/gae.2018.14.6.519.

Zamanian, M., Kolahchi, R. and Bidgoli, M.R. (2017), "Agglomeration effects on the buckling behaviour of embedded concrete columns reinforced with SiO2 nano-particles", *Wind Struct.*, **24**(1), 43-57. https://doi.org/10.12989/was.2017.24.1.043.

Zarei, M.S., Kolahchi, R., Hajmohamm, M.H. and Maleki, M. (2017), "Seismic response of underwater fluid-conveying concrete pipes reinforced with SiO2 nanoparticles and fiber reinforced polymer (FRP) layer", *Soil Dyn. Earthq. Eng.*, **103**, 76-85. https://doi.org/10.1016/j.soildyn.2017.09.009.

Zhang, F., Lu, Y., Li, S. and Zhang, W. (2018), "Eccentrically compressive behaviour of RC square short columns reinforced with a new composite method", *Steel Compos. Struct.*, **27**(1), 95-108. https://doi.org/10.12989/scs.2018.27.1.095.

JS